Supplemental Material: Operator scaling dimensions and multifractality at measurement-induced transitions

CONTENTS

I. EQUILIBRATION TIME

In this section, we describe our numerical method of computing the free-energy of the implicit statistical mechanics model describing MIPTs in the generic models. We introduce a method to cleanly distinguish bulk and boundary contributions to the free-energy.

The entropy of the measurement record F can be viewed as an average of the logarithm of the probability of a given trajectory, i.e., $F = -\sum_{\mathbf{m}} p_{\mathbf{m}} \ln p_{\mathbf{m}} = -\sum_{\mathbf{m}} \langle \ln p_{\mathbf{m}} \rangle$. Here, the expectation value is taken over an ensemble where each trajectory is weighted by its Born probability. Since the probability of a given trajectory depends on the product of the Born probabilities of all the measurements we can write

$$F = -\sum_{i=1}^{N_{\text{meas}}} \langle \ln p(m_i | m_{i-1}, ..., m_1) \rangle, \tag{1}$$

where $p(m_i|m_{i-1},...,m_1)$ is the conditional probability of the set of measurement outcomes m_i given the previous series of measurement outcomes. This result shows that we can perform a Monte Carlo sampling of the Born probabilities obtained during the simulation to compute F. The entropy is quite sensitive to the initial conditions at early times as we now describe.

To compute the entropy density, we record the entropy accumulated as a function of time, $F(t)$, and obtain the density from the slope of the linear fit of the infinite time limit entropy density of the measurement record $F(t\to\infty)/L$ vs t. As an integral, this quantity, at late times takes the form $F(t\to\infty)/L = F^{\rm bdry} + tF^{\rm bulk}$ where $F^{\rm bdry}$ comes from the choice of initial state and $F^{\rm bulk}$ comes from the steady state wave function. As a result, $F(t\to\infty)/tL = F^{\rm bdry}/t + F^{\rm bulk}$ indicating a convergence of $1/t$ as indicated in Fig. 1a by the solid lines. To uncover when the boundary effects are saturated, we can take two different initial states, a Haar random initial state and a random product state, and compute $\Delta F(t) \equiv F^{\rm Haar}(t) - F^{\rm product}(t)$ which saturates when the boundary effects saturate; we observe exactly this in Fig. 1b. Once saturation is achieved, we can effectively deduce that the wave function has reached the steady state and the average (green) is saturated. This saturation criteria agrees well with the half-cut entropy shown in the inset of Fig. 1a, and we conservatively obtain $\tau_{\rm Haar} \sim \tau_{\rm product} \lesssim 2L$ suggesting we should wait a time $\tau > 2L$ before we begin recording the entropy of the measurement record. For our data we have chosen $\tau = 4L$ and recorded the data for an additional time $t_f = 24L$, where one time step consists of either an even or odd layer of gates and a layer of measurements. To further improve results, after averaging over the random Haar and product initial states separately, the results are averaged together. The error in the entropy density of the measurement record is estimated by computing the entropy density for individual trajectories and performing a bootstrap analysis [1]. The two initial states are bootstrapped separately over 1000 samples and their errors are combined using

$$\sigma = \frac{1}{2}\sqrt{\sigma^2_{\rm Product} + \sigma^2_{\rm Haar}}. \tag{2}$$

II. ANISOTROPY PARAMETER

In this section, we describe the arguments based on conformal invariance that allow us to efficiently extract the anisotropy parameter at critical points of random circuits with measurements in 1+1 dimensions.

To estimate the area, $A = \alpha tL$, that arises in the free energy density, it is necessary to calculate the anisotropy parameter, α, that relates space and time, i.e., $L = \alpha t$. This parameter can be estimated by comparing the correlation functions along the space and time directions as we describe below. Using the conformal mapping $z' = f(z) = \frac{L}{2\pi}\ln z$ (see Fig. 2), we can relate the correlation functions on the infinite cylinder, $g'(z'_1, z'_2)$, to correlation functions on the plane, $g(z_1, z_2)$, through

$$g'(z'_1, z'_2) = |f'(z_1)|^{-\Delta}|f'(z_2)|^{-\Delta} g(z_1, z_2), \tag{3}$$

where Δ is the conformal dimension. For a 1+1 dimensional CFT,

$$g(z_1, z_2) = \frac{1}{|z_1 - z_2|^{2\Delta}} \tag{4}$$

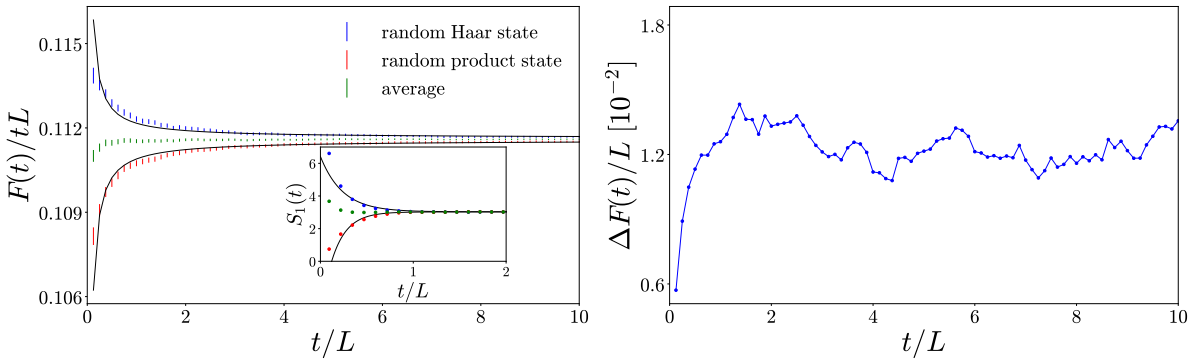

(a) (b)

FIG. 1. (a) Average entropy density of the measurement record after a time t. Due to boundary effects, the entropy density of the measurement record averaged separately over random Haar and random product initial states saturates slowly to their common asymptotic value. To limit these effects, we wait an equilibration time $\tau = 4L$ before recording the entropy of the measurement record and then average the two results together. Data is shown for $L = 16$, $p = 0.17$ and 25 000 samples. In the inset, we show that this saturation criteria agrees well with the half-cut von Neumann entanglement entropy, $S_1(t)$. (b) The difference between the entropy of the measurement records $\Delta F(t) = F^{\text{Haar}}(t) - F^{\text{product}}(t)$.

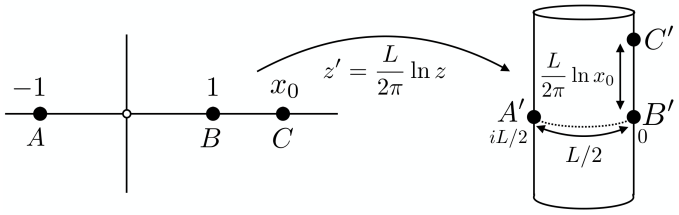

FIG. 2. The conformal mapping from a plane to a cylinder.

and after applying the transformation to Eq. (4) we have

$$g'(z_1', z_2') = \left(\frac{\pi}{L}\right)^{2\Delta} \frac{1}{\left|\sinh\left[\frac{\pi}{L}\left(z_1' - z_2'\right)\right]\right|^{2\Delta}}. \tag{5}$$

We can extract α from the ratio of the correlation functions

$$g'_{\text{space}} = g'(0, iL/2) = \left(\frac{\pi}{L}\right)^{2\Delta} \tag{6}$$

$$g'_{\text{time}} = g'(0, \alpha t) = \left(\frac{\pi}{L}\right)^{2\Delta} \left(\frac{2e^{\pi\alpha t/L}}{e^{2\pi\alpha t/L} - 1}\right)^{2\Delta} \tag{7}$$

$$\frac{g'_{\text{time}}}{g'_{\text{space}}} = \left(\frac{2e^{\pi\alpha t/L}}{e^{2\pi\alpha t/L} - 1}\right)^{2\Delta}. \tag{8}$$

To eliminate the dependence on Δ, we look for the matching time, t_*, at which the space and time correlation functions acquire the same value. Setting $g'_{\text{time}}/g'_{\text{space}} = 1$ in Eq. (8), the resulting

quadratic equation can be solved for the anisotropy parameter

$$\begin{aligned} & e^{2\pi\alpha t_*/L} - 2e^{\pi\alpha t_*/L} - 1 = 0 \\ \implies & \alpha = \ln\left(1+\sqrt{2}\right)\frac{L}{\pi t_*}. \end{aligned} \tag{9}$$

To compute this numerically, we calculate the mutual information between two initially locally entangled reference qubits. We run the unitary-measurement dynamics out to $\tau_1 = 4L$, measure site x_1 and entangle this site with a reference qubit. We then run the dynamics out to τ_2, measure site x_2 and entangle this site with another reference qubit. After this second event, we follow the mutual information $I_{12}(x_1, x_2, \tau_1, \tau_2)$ between the two reference qubits as a probe of the order parameter correlations. We use a space like separation of $\delta x = |x_2 - x_1| = L/2$ with $\delta\tau = 0$ to determine g'_{space} and time like separation of $\delta\tau = \tau_2 - \tau_1$ with $\delta x = 0$ to determine g'_{time}.

III. LYAPUNOV EXPONENTS

In this section, we describe a procedure that only requires storing a set of vectors that are iterated upon in order to compute the Lyapunov exopnents.

The Lyapunov exponents of the transfer matrix can be related to the free energy densities that are used in the calculation of the scaling dimensions of operators in the theory. However, working with the full transfer matrix becomes exponentially difficult in the system size and an alternative approach is needed.

We are interested in characterizing the large m behavior of the application of i.i.d. random transfer matrices $\mathcal{T}_j \in \mathbb{C}^{d\times d}$ to a vector $|v_0\rangle \in \mathbb{C}^d$ with $j = 1, 2, \ldots, m$. This evolution can be described by the recurrence

$$|v_0^{(j)}\rangle = \mathcal{T}_j |v_0^{(j-1)}\rangle, \qquad j = 1, 2, ..., m \tag{10}$$

for some initial normalized vector $|v_0\rangle$. The randomness of the matrices $\mathcal{T}_j$ implies the choice of the probabily measure on $\mathbb{C}^{d\times d}$. The large m behavior can be characterized by considering the leading Lyapunov exponent found by the Furstenberg method

$$\lambda_0(L) = \lim_{m\to\infty} \frac{1}{m} \mathbb{E} \log \left\| |v_0^{(m)}\rangle \right\| \tag{11}$$

where $\mathbb{E}$ denotes the expectation over the random matrices. Equation (11) is independent of the initial vector $|v_0\rangle$ for almost all realizations of the matrices $\mathcal{T}_j$. An alternative definition that makes the independence on $|v_0\rangle$ explicit is

$$\lambda_0(L) = \lim_{m\to\infty} \frac{1}{m} \mathbb{E} \log \left\| \prod_{j=1}^{m} \mathcal{T}_j \right\| \tag{12}$$

where the matrix norm is the 2-norm, so that $\left\|\prod_{j=1}^m \mathcal{T}_j\right\|$ is the largest singular value of $\prod_{j=1}^m \mathcal{T}_j$. The average free energy per site is related to the leading Lyapunov exponent by

$$f(L) = -\frac{1}{\alpha L}\lambda_0(L). \tag{13}$$

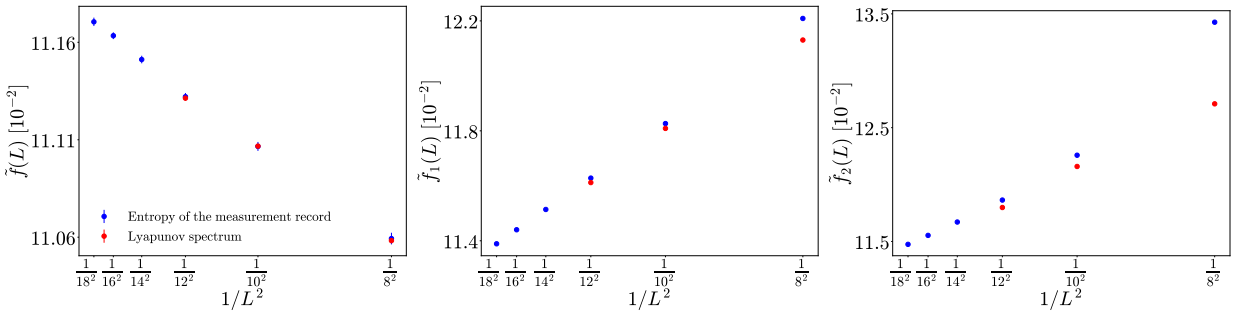

(a) (b) (c)

FIG. 3. Comparison of the free energy density obtained using the entropy of the measurement record based on the orthogonal vectors with the free energy density obtained using the Lyapunov spectrum based on the singular values of the transfer matrix. At small system sizes, the Gram-Schmidt orthogonaliztion procedure quickly zeros out the higher order orthogonal vectors making it difficult to sample at late times. The tilde in the free energy density denotes that α is not taken into account in the area.

Similarly, the generalized free energies can be related to the higher order Lyapunov exponents through $f_i(L) = -\frac{1}{\alpha L}\lambda_i(L)$. In order to numerically compute λ_i, we can consider of a set of n orthogonal vectors $\{|v_k\rangle\}, k = 0, 1, \ldots, n-1$ and iteratively apply the transfer matrices, $\mathcal{T}_j$. After each application of $\mathcal{T}_j$, the set must be orthogonalized again. In Fig. 3 we show that the value of the free energy density obtained from the Lyapunov spectrum approaches that from the entropy of the measurement record. At small system sizes, the Gram-Schmidt orthogonalization procedure quickly zeros out the orthogonal vectors making it difficult to sample at late times. Note that for the vectors $k > 0$, the entropy of the measurement record, F_k, must be slightly modified to account for the orthogonalization procedure and is given by

$$F_k = -\sum_{j=1}^{m} \ln \left\| P^{(j)}_{\mathrm{GS},k} P^{(j)}_{\mathrm{M}} |v_k^{(j-1)}\rangle \right\|^2, \tag{14}$$

where $P^{(j)}_{\mathrm{GS},k}$ is a projector from the Gram-Schmidt process and $P^{(j)}_{\mathrm{M}}$ is a projector onto the meaurement outcomes in $\mathcal{T}_j$.

IV. HAAR RANDOM CIRCUIT

In this section, we estimate the anisotropy parameter for the Haar random circuit and use it to compute the effective central charge and scaling dimensions of operators in theory. We also show evidence of multifractal scaling at the critical point.

We can compute the anisotropy parameter for the Haar random circuit using the procedure described in Sec. II. The correlation functions along the space and time directions are shown in Fig. 4. Numerically computing the correlation functions shows that the matching time is between $t = 5L/16$ and $t = 6L/16$. Performing a linear interpolation

$$t_* = t_5 + [I_{\mathrm{space}} - I(t_5)] \frac{t_6 - t_5}{I(t_6) - I(t_5)} \tag{15}$$

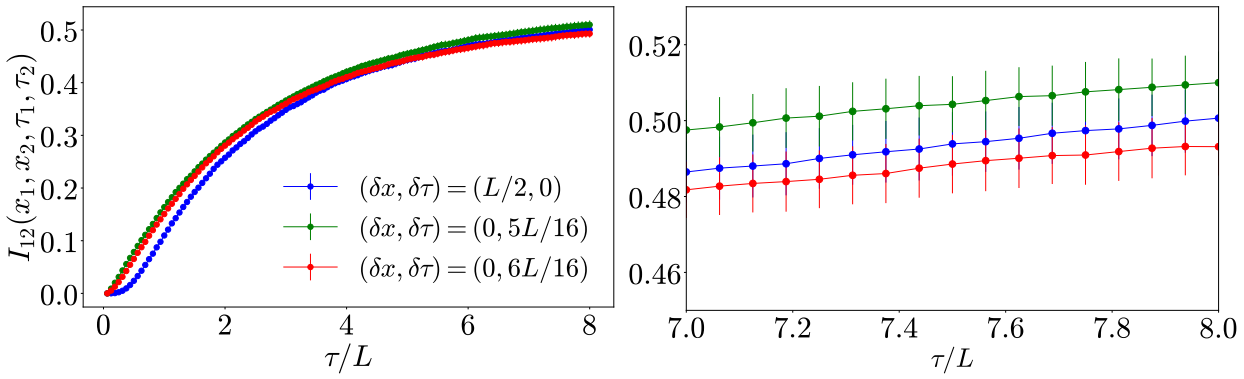

(a) (b)

FIG. 4. Haar model space and time correlation functions at $p_c = 0.170$ for $L = 16$. The matching time, t_*, lies between $t = 5L/16$ and $t = 6L/16$. Using a linear interpolation we estimate the true matching time to be $t_* = 5.55$ and, therefore, $\alpha = 0.81(9)$.

which gives $t_* = 5.55$ and $\alpha = 0.81 \pm 0.09$ with the error bar spanning the range $t_* \in [t_5, t_6]$.

This anisotropy parameter can be incorporated with the results of the free energy density scaling shown in Fig. 5 to estimate $c_{\text{eff}} = 0.25(3)$. Note that we have introduced a tilde into the notation of the free energy density, $\tilde{f}$, to indicate that it does not contain α in the area. The fit to the slope of $\tilde{f}(L)$ in the inset is given by $m_0(L) = -0.105 + \frac{0.958}{L^2}$. We can also compute the critical exponents, x_i^{typ}, from the differences of the generalized free energy densities as shown in Fig. 6. Performing the double fitting procedure and incorporating α into the result we find $x_1^{\text{typ}} = 0.14(2)$, $x_2^{\text{typ}} = 0.18(2)$, $x_3^{\text{typ}} = 0.23(3)$. The fits in the inset are given by $m_1(L) = 0.703 + \frac{1.30}{L^2}$, $m_2(L) = 0.924 + \frac{15.5}{L^2}$, and $m_3(L) = 1.14 + \frac{25.9}{L^2}$. Additionally, we find evidence of multifractality at the critical point based on the data collapse of $H(s)$ as well as the scaling of the cumulants of $\ln G_1(t)$, see Fig. 7.

V. DUAL UNITARY

In this section, we determine the critical point of the dual unitary model using the entanglement transition order parameter. At the critical point, we verify that $\alpha = 1$ and use it to compute the effective central charge and scaling dimensions of operators in theory.

As argued in the main text, the transition in the dual unitary model lies in the same universality class as that of the generic Haar model and is used to provide a more accurate estimate of the quantities calculated as it constrains $\alpha = 1$.

The dual unitary circuit model we consider consists of 2-qubit gates of the form [2]

$$U = e^{i\phi}(u_+ \otimes u_-) \cdot V[J] \cdot (v_- \otimes v_+) \tag{16}$$

where $\phi, J \in \mathbb{R}, u_\pm, v_\pm \in \text{SU}(2)$ and

$$V[J] = \exp[-i\left(\frac{\pi}{4}\sigma^x \otimes \sigma^x + \frac{\pi}{4}\sigma^y \otimes \sigma^y + J\sigma^z \otimes \sigma^z\right)]. \tag{17}$$

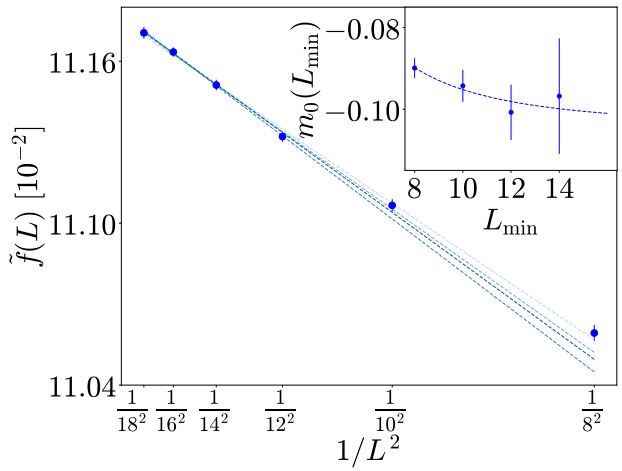

FIG. 5. The free energy density of the Haar model shows the expected $1/L^2$ scaling. Using the double fitting procedure described in the main text we can extract c_{eff} from the slope of the free energy density. For the Haar model we find $c_{\text{eff}} = 0.25(3)$, in agreement with the dual unitary result placing the two models into the same universality class. The tilde in the free energy density, $\tilde{f}$, indicates that α has not been taken into account in the area. Darker blue indicates larger values of $L_{\min} = 8 \to 14$.

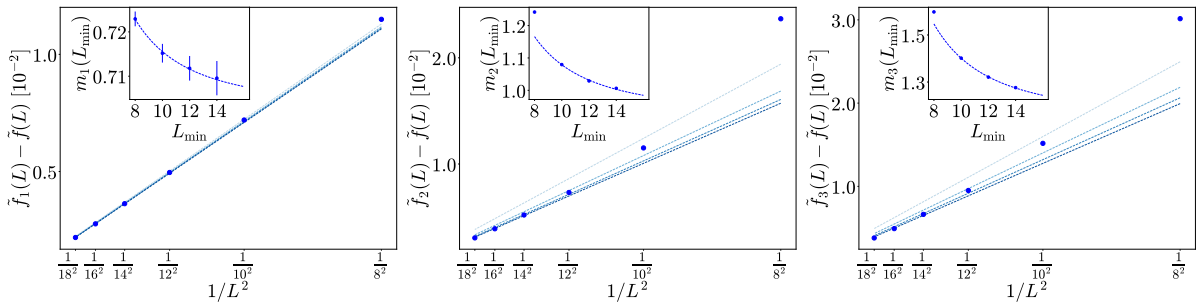

(a) (b) (c)

FIG. 6. Scaling of the generalized free energies in the Haar model. The differences between the free energy densities can be related to the scaling dimension, x_i^{typ}, of operators in the theory. In the figure, the tilde, e.g. $\tilde{f}_i$, denotes that we have no included the anisotropy parameter into the area and it will be introduced in the final result. Using a similar double fitting procedure as for the effective central charge, the typical values of the first three scaling dimensions are estimated to be $x_1^{\text{typ}} = 0.14(2), x_2^{\text{typ}} = 0.18(2), x_3^{\text{typ}} = 0.23(3)$. Darker blue indicates larger values of $L_{\min} = 8 \to 14$.

With this choice, U is unitary in both the space and time directions, i.e., $U^\dagger U = \tilde{U}^\dagger \tilde{U} = \mathbb{1}$ where

$$\langle k| \otimes \langle l|\tilde{U}|i\rangle \otimes |j\rangle = \langle j| \otimes \langle l|U|i\rangle \otimes |k\rangle. \tag{18}$$

In the numerical simulations we choose ϕ, J uniformly from $[0, 2\pi)$. To find the critical point we look at the order parameter as a function of the measurement probability p. This is the best measure of the critical point since there is a strong even/odd effect in the tripartite mutual information ($\mathcal{I}_3$) data. In Fig. 8a we see a clear crossing of the order parameter at $p_c = 0.14(1)$. Using this critical point we can estimate the anisotropy parameter α by measuring correlation functions along the space and time dimensions as described in Sec. II. Numerically computing the correlation functions

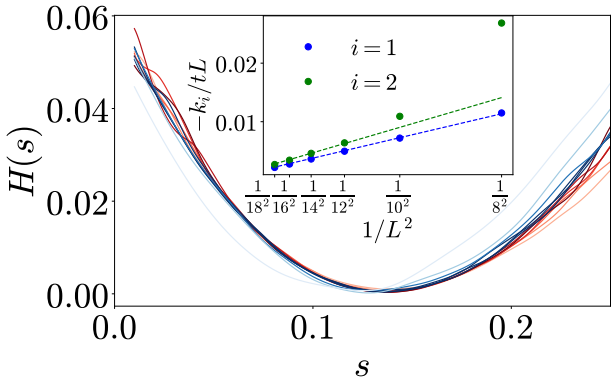

FIG. 7. The scaling collapse of the data onto a universal multifractal scaling function $H(s)$ demonstrates multifractality at the critical point of the Haar transition and corresponds to a continuum of critical exponents. Data is shown for the Haar model where darker red indicates larger system sizes ($L = 8 \to 18, t = 24L$) and darker blue indicates later times ($t = 3L \to 24L, L = 16$). (inset) The first two cumulants k_i of $\ln G_1(t)$ divided by tL show the expected $1/L^2$ behavior.

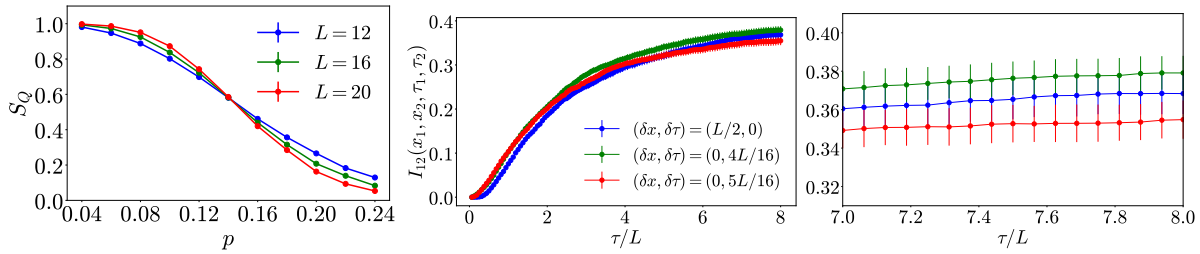

(a) (b) (c)

FIG. 8. (a) Dual unitary order parameter S_Q as a function of the measurement probability, p. The critical point is indicated by the crossing at $p_c = 0.14(1)$. (b) and (c) Dual unitary space and time correlation functions at $p_c = 0.140$ for $L = 16$. The matching time, t_*, at which the space and time correlation functions coincide lies between $t = 4L/16$ and $t = 5L/16$. Using a linear interpolation we can estimate the true matching time to be $t_* = 4.44$ and, therefore, $\alpha = 1.0(1)$ in agreement with the expectation that $\alpha = 1$.

shows that the matching time is between $t = 4L/16$ and $t = 5L/16$, see Figs. 8b and 8c. We can get a better estimate of this time by performing a linear interpolation

$$t_* = t_4 + [I_{\text{space}} - I(t_4)] \frac{t_5 - t_4}{I(t_5) - I(t_4)} \tag{19}$$

which gives $t_* = 4.44$ and $\alpha = 1.0 \pm 0.1$ with the error bar spanning the range $t_* \in [t_4, t_5]$. This result is in agreement with our expectation that $\alpha = 1$ by the construction of the gates. In what follows, we take α to be exactly one, thereby, eliminating the parameter from the calculations and reducing the error bars in the estimates of all quantities for this model.

The free energy density is shown in the main text where we extract the effective central charge, $c_{\text{eff}} = 0.24(2)$. This value is consistent with the result for the Haar random circuit (see below) but with much smaller error bars. Additionally, in the main text, we estimated the scaling dimensions, x_i^{typ}, of operators in the theory by computing the differences between the free energy densities. The

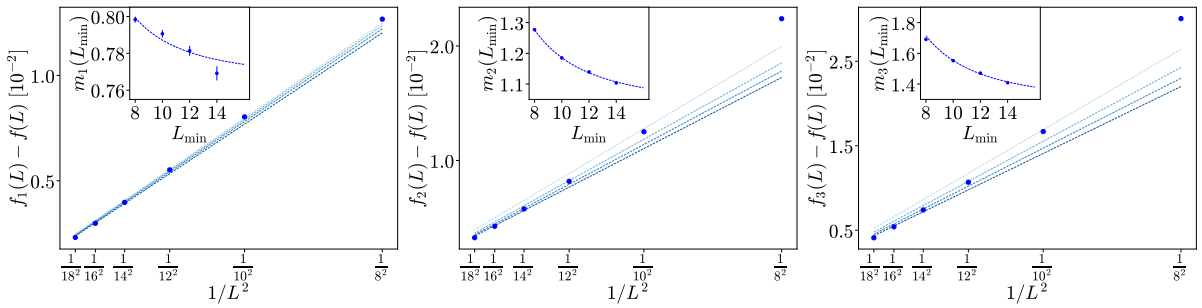

(a) (b) (c)

FIG. 9. Scaling of the generalized free energies in the dual unitary model. The differences between the free energy densities can be related to the scaling dimension, x_i^{typ}, of operators in the theory. Using a similar double fitting procedure as for the effective central charge, the typical values of the first three scaling dimensions are estimated to be $x_1^{\text{typ}} = 0.122(1), x_2^{\text{typ}} = 0.163(1), x_3^{\text{typ}} = 0.202(1)$. Darker blue indicates larger values of $L_{\min} = 8 \to 14$.

system size dependence used for the double fitting procedure is shown in Fig. 9 and the equation for each of the fits in the insets are given by $m_1(L) = 0.766 + \frac{2.16}{L^2}$, $m_2(L) = 1.03 + \frac{16.1}{L^2}$, and $m_3(L) = 1.27 + \frac{28.5}{L^2}$.

VI. STABILIZER CIRCUITS

In this section, we estimate the anisotropy parameter and c_{eff} for the 1+1D random Clifford model [3].

In the case of a stabilizer circuits, it turns out one can compute the entropy of the measurement record for a fixed circuit without any sampling by simply counting the number of deterministic measurement outcomes N_{det} out of all measurements

$$F = (N_{\text{meas}} - N_{\text{det}}) \log 2, \tag{20}$$

which follows from the dynamical update rules for stabilizer circuits [4].

In Fig. 10, we show numerical data we have used to estimate α up to system sizes $L = 128$. In Fig. 10a, we show the mutual information between two initially locally entangled reference qubits for space and time-like separations between the reference qubits.

To perform the time-like interpolation we use $\delta_x = 0$ with the separation $\delta\tau = \tau_2 - \tau_1 = 6L/16$ and $7L/16$ that is close to the point where $r = 1$. As shown in Fig. 10b, at our largest value of $L = 128$, we find

$$\alpha = 0.616 \pm 0.021 \text{ (stat.)} \pm 0.0037 \text{ (interp.)} = 0.616 \pm 0.025 \tag{21}$$

We have estimated the interpolation error arising from a linear interpolation approximation using

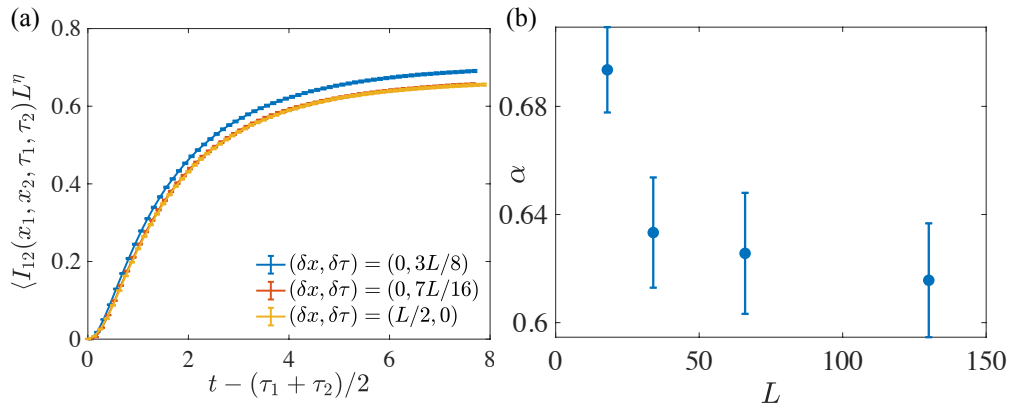

FIG. 10. (a) Scaled mutual information between two reference qubits for different space and time like separations at $p = 0.1596$ for $L = 128$ with the percolation value $\eta = 5/24$. We averaged over $12 \cdot 10^5$ circuits. (b) Extracted $\alpha(p, L)$ for $p = 0.1596$ up to $L = 128$.

the formulas

$$r(\tau) \approx 1 - 2\sqrt{2}\pi\alpha\Delta(\tau - t_*) + \pi^2\alpha^2\Delta(1 + 4\Delta)(\tau - t_*)^2, \tag{22}$$

$$\frac{t_*}{L} = \frac{\tau_1}{L} + \frac{[1 - r(\tau_1)]\delta\tau}{[r(\tau_2) - r(\tau_1)]L} + \text{Error} \approx 0.4579 \pm 0.0028 \text{ (interp)}, \tag{23}$$

where we used the estimates $t_* = 0.4579$, $\alpha = 0.616$, and $\Delta = 0.1042$ to approximate the error term arising from the quadratic correction to $r(\tau)$.

The anisotropy parameter as we have defined it will also have corrections due to uncertainty in p_c, which leads to the finite size scaling form $\alpha(L/\xi)$, where $\xi \approx X_\pm/|p - p_c|^\nu$. We previously obtained a quantitative estimate for the prefactor $X_\pm = 0.18/0.12$ above and below the critical point [5], which implies that with the currently available precision on $p_c = 0.1593(5)$, the expected correlation length is several hundred to several thousand lattice sites within this uncertainty window. Numerically, we do not observe any statistically significant dependence of $\alpha(p)$ over this range of p.

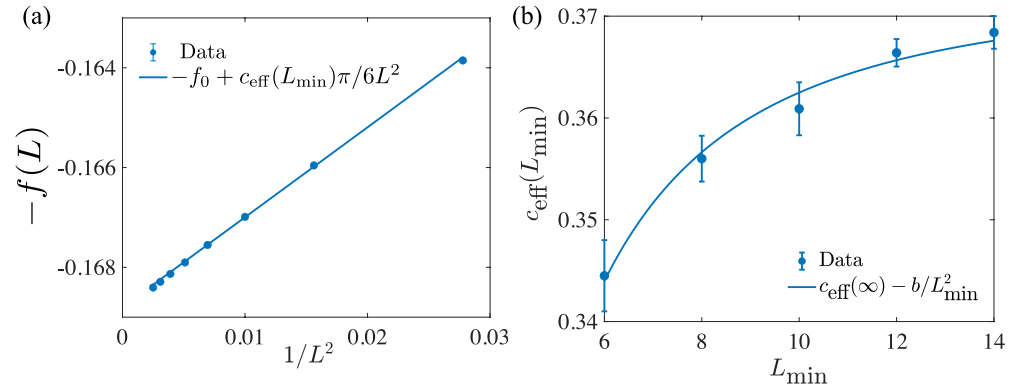

FIG. 11. (a) Average entropy density of the measurement record vs $1/L^2$ for $L_{\min} = 6$. (b) Dependence of the extracted slope vs $1/L^2$ as a function of the cutoff $L_{\min}$.

With the anisotropy parameter calibrated, we can now numerically compute the average free energy of the underlying statistical mechanics model. The numerical results are shown for $p = 0.1596$ in Fig. 11a, where we see the predicted scaling behavior with L. By successively removing smaller sizes $L < L_{\min}$ from the fit we can obtain a sequence of values $c_{\text{eff}}(L_{\min})$. Performing the fit

$$c_{\text{eff}}(L_{\min}) = c_{\text{eff}}(\infty) - \frac{b}{L_{\min}^2}, \tag{24}$$

allows a reliable method to extract the asymptotic value $c_{\text{eff}}(\infty)$ [6]. The results of this analysis are shown in Fig. 11b. To determine the variations with $c_{\text{eff}}(\infty)$ for different values of p we have scanned several values near the critical point and find the maximum occurs near $p = 0.1596$, which we use as our estimate of the critical point (see Table I). The variation with p throughout this region is close to the uncertainty in the fits.

TABLE I. Extracted value of c_{eff} for different values of p near the estimated critical point.

p	0.1594	0.1596	0.1598
$c_{\text{eff}}(\infty)$	0.3716 ± 0.0007	0.3729 ± 0.0016	0.3705 ± 0.0009

Overall, we obtain the estimate for c_{eff} including statistical errors and the error in the anisotropy parameter

$$c_{\text{eff}}^s = 0.3729 \pm 0.0016 \text{ (stat.)} \pm 0.016 \text{ (anis.)} = 0.373 \pm 0.018 \tag{25}$$

VII. PURIFICATION EXPONENTS IN STABILIZER CIRCUITS AND MINIMAL-CUT PERCOLATION MODELS

In this section, we compare the order parameter exponent between the minimal-cut/Haar-Hartley percolation universality class and the stabilizer circuit universality class. We also describe the numerical method we used to more accurately extract the order parameter exponent for the stabilizer circuit models.

A. Purification exponents

The von Neumann entropy dynamics $S(\rho)$ of a mixed state $\rho = K_{\boldsymbol{m}}\rho_0 K_{\boldsymbol{m}}^\dagger / p_{\boldsymbol{m}}$ evolved under a stabilizer circuit has qualitatively the same behavior as the Hartley entropy $S_0(\rho)$ in the Haar random model. The latter of which has an exact mapping to a percolation problem through the minimal-cut procedure developed in Ref. [7]. For this reason, we first benchmark our method on the Haar-Hartley percolation model. In both models, the relevant entropy changes in discrete steps of $\log 2$. At the critical point, we have found that the late time decay rate for the relevant entropy changing from $n \log 2$ to a value $< n \log 2$ saturates to a constant. This behavior is consistent with

a late time exponential decay behavior for the probability of a circuit maintaining entropy $n \log 2$. We define the average quantity

$$\Delta\lambda_n(t) = \frac{1}{\alpha L} \frac{\#\text{ Circuits for which } S(\rho) \text{ goes from } n\log 2 \text{ to a value} < n\log 2 \text{ at time } t}{\#\text{ Circuits with } S(\rho) = n\log 2 \text{ at time } t-1}, \quad (26)$$

Here, α is the anisotropy parameter. In the Haar-Hartley percolation model $\alpha = 1$. For stabilizer circuits, we focus on the random dual Clifford model where each two-site gate is chosen uniformly randomly from the set of dual-unitary Clifford gates. This model is expected to have $\alpha = 1$ for each circuit, which we have verified numerically using the method described in the previous section. This property makes it convenient for numerical analysis similar to the dual-unitary Haar random model.

To connect this quantity $\Delta\lambda_n(t)$ to more conventional observables at the critical point, we note that, if we start with a mixed state with one bit of entropy, then

$$\Delta\lambda_1(t) = -\frac{1}{\alpha L \langle S(\rho)\rangle} \frac{\Delta\langle S(\rho)\rangle}{\Delta t}, \quad (27)$$

is just the logarithmic time derivative of the entropy of the mixed state. Within the conformal field theory picture for percolation and the stabilizer circuit models, we have the relation [8]

$$\lim_{t\to\infty} \Delta\lambda_1(t) = \frac{2\pi}{L^2} x_1, \quad (28)$$

where x_1 is the order parameter exponent. Our definition of $\Delta\lambda_n$ allows us to generalize this exponent to an infinite family of "purification" exponents. This spectrum of exponents serves as a more precise comparison between the stabilzer circuit and Haar-Hartley percolation universality class.

Our numerical results for λ_n for $n = 1$ and $n = 2$ are summarized in Table II. For the random Clifford model using these methods, we find $x_1^p = 0.120(5)$ and $x_2^p = 0.240(5)$ with an uncertainty limited mostly by the uncertainty in the anisotropy parameter. In this case, we observe a significant difference from Haar-Hartley percolation values only for x_2^p. On the other hand, for the random dual Clifford model, we observe that it also has a significant difference in the value of x_1^p due to the smaller numerical uncertainties in the estimated value. This large relative difference in x_1^p between the two models is a strong indication that they lie in separate universality classes.

TABLE II. The first two purification exponents in the random dual Clifford model and the Haar-Hartley percolation model. To our knowledge, x_2^p has not been previously studied in percolation.

	Clifford	Dual Clifford	Haar-Hartley Exact	Haar-Hartley Numerics
x_1^p	0.120(5)	0.111(1)	$5/48 = 0.1042\ldots$	0.104(1)
x_2^p	0.240(5)	0.230(1)	???	0.366(3)

B. Numerical method

Our numerical method used for extracting the purification exponents is illustrated in Fig. 12 for the Haar-Hartley percolation model and the random dual Clifford model. To improve the numerical

precision for x_1^p, we choose different initial conditions whereby the decay rate approaches its late time plateau from either above or below the plateau value. By averaging these two results, we can reduce systematic errors in our numerical estimate of the plateau value.

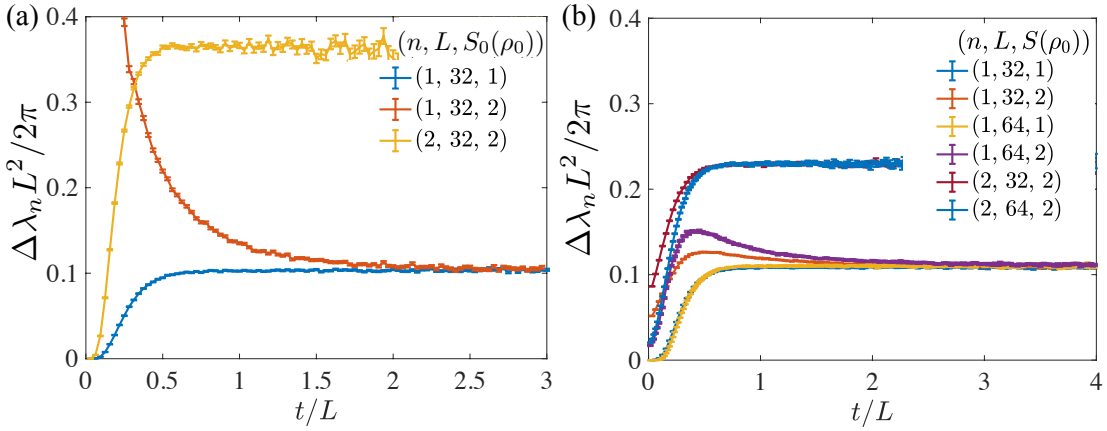

FIG. 12. (a) Scaled purification rate for the Hartley entropy of the reference system in the Haar random model at the critical point $p = 0.5$. The decay rate from entropy n to $< n$ allows us to extract the purification exponent x_n^p from the late time plateau. $x_1^p = x_1^{(1)}$ coincides with the order parameter exponent. (b) Scaled purification rates for the entropy of the reference system in the random dual Clifford model at $p = 0.205 \approx p_c$.

For the Haar-Hartley percolation model shown in Fig. 12a, we took an initial state with Hartley entropy $S_0(\rho) = 2$ or 1, fully scrambled the system with a Haar random circuit, and then turned on the measurements at the critical rate $p = 0.5$. In the percolation mapping, the scrambling layer corresponds to taking a fully connected bottom boundary. To compute $S_0(\rho)$, we used the max-flow/min-cut algorithm applied to a percolating network. With this method, we were able to extract a value of x_1^p that is with 1% of the known percolation value of 5/48. To our knowledge, the exact values of x_n^p for $n > 1$ are not known within the minimal cut picture for the Haar-Hartley entropy. We provide the first numerical estimate of x_2^p here.

For the random dual Clifford model shown in Fig. 12b, the boundary conditions were chosen in a similar manner to the Haar-Hartley model; however, to improve the rate at which the $S(\rho_0) = 2$ initial condition approaches the plateau, we scrambled the initial condition with a depth L random circuit that also includes measurements at rate $p = p_c/1.25$. As a result, the quench to the critical point is less dramatic compared to a fully unitary scrambling circuit. For the initial condition $S(\rho_0) = 1$, the scrambling layer was taken to be a depth $2L$ random Clifford circuit in 1D with no measurements. The critical point $p_c = 0.205(1)$ for the random dual Clifford model was obtained using the order parameter crossing method described in our previous work [9]. The extracted value of p_c strongly violates the Hashing bound for a depolarizing channel that was conjectured to be a relevant bound on the critical measurement rate $p_c \leq 0.1893$ for unitary-projective circuits in one dimension [10].

VIII. EFFECTIVE CENTRAL CHARGE IN THE LARGE ONSITE HILBERT SPACE DIMENSION LIMIT

In this section, we derive exact expressions for the effective central charge $c_{\rm eff}$ of the MIPT of monitored qudit circuits for both Haar and Clifford random gates, in the limit $d \to \infty$ where d is the dimension of the onsite Hilbert space. Note that, as already recalled in a footnote in the introductory part of the main text, $c_{\rm eff}$ is *not* related to the prefactor of the logarithmic scaling with subsystem size of the entanglement entropy at criticality, which is instead related to the scaling dimension of boundary condition changing operators [11, 12].

A. Haar case

In the case of Haar gates drawn from the unitary group $U(D = d^2)$, we follow Refs. [12, 13] (see also [11, 14, 15]) to map the anneal averaged replicated partition functions $\bar{Z}_r = \sum_{\mathbf{m}} p_{\mathbf{m}} Z^r_{\mathbf{m}}$ onto an effective statistical model (recall, $Z_{\mathbf{m}} = p_{\mathbf{m}}$ in our formulation), whose degrees of freedom are permutations $g_i \in S_{1+r}$. Formally, this follows from the so-called Schur-Weyl duality, which states that the permutation group S_{1+r} and the unitary group $U(D)$ act on $(\mathbb{C}^D)^{\otimes(1+r)}$ as a commuting pair. In the limit $d \to \infty$, the statistical mechanics model simplifies dramatically, and reduces to a Potts model with $|S_{r+1}| = (r+1)!$ states. In the replica limit $r \to 0$, this gives a MIPT in the percolation universality class [12, 13].

For a finite number of replicas r, this Potts model has a phase transition described by a CFT with central charge

$$c(r) = 1 - \frac{6}{x(x+1)} \text{ with } x + 1 = \frac{\pi}{\arccos \frac{\sqrt{(r+1)!}}{2}}. \tag{29}$$

In the replica limit, we have $c(r \to 0) = 0$, and we can use this expression to evaluate the effective central charge

$$c_{\rm eff}^{H,d\to\infty} = \lim_{r\to 0} \frac{dc}{dr} = \frac{5\sqrt{3}(1-\gamma)}{4\pi} \simeq 0.291367\ldots \tag{30}$$

with $\gamma \simeq 0.577216\ldots$ Euler's constant.

B. Clifford case

We now turn to a similar calculation in the case of Clifford gates. The full derivation of the corresponding statistical mechanics model (for the Clifford measurement-induced phase transition and random tensor networks [11] with Clifford tensors) with on-site Hilbert space dimension $d = p^n$ and p prime will be reported elsewhere [16], where it will also be shown that its symmetry depends explicitly on p, implying universality of transitions depending on p. Here we simply emphasize the key ingredients to compute $c_{\rm eff}$ in the limit of large onsite Hilbert space. In order to average over Clifford gates to derive a statistical model, we will need a generalization of the Schur-Weyl duality. Let $D = d^2$ with $d = p^n$ and p prime. We are interested in the Clifford group $\mathcal{C}$, which is a finite

subgroup of the unitary group $U(D)$ acting on $r+1$ replicas. In general, the "commutant" $\mathcal{F}_r$ of $\mathcal{C}$ acting on this space will be larger than the symmetric group S_{r+1}, and was recently analyzed in Ref. [17]. In order to analyze the structure of this algebraic object, note that the tensor space $V = (\mathbb{C}^D)^{\otimes(r+1)}$ can be decomposed onto the irreps V_λ of $\mathcal{C}$ as $V = \bigoplus_\lambda d_\lambda V_\lambda$. The dimension of the commutant $\mathcal{F}_{r+1}$ of the Clifford group $\mathcal{C}$ acting on this replicated space is $|\mathcal{F}_{r+1}| = \sum_\lambda d_\lambda^2$, and can be computed as follows. Let $\chi_V(U) = \text{tr } U^{\otimes(1+r)}$ be the character of the representation $(\mathbb{C}^D)^{\otimes(1+r)}$ of the Clifford group $\mathcal{C}$, where $U \in \mathcal{C}$ is a Clifford gate acting on $\mathbb{C}^D$. Introducing the inner product between characters $\langle \chi_1, \chi_2 \rangle = \frac{1}{|\mathcal{C}|} \sum_{U \in \mathcal{C}} \overline{\chi_1(g)} \chi_2(g)$, we have $\langle \chi_V, \chi_V \rangle = \sum_\lambda d_\lambda^2$. The dimension of the commutant $\mathcal{F}_{r+1}$ of the Clifford group – which replaces the symmetric group S_{r+1} in the statistical mechanics model – is thus given by

$$|\mathcal{F}_{r+1}| = \frac{1}{|\mathcal{C}|} \sum_{U \in \mathcal{C}} |\text{tr } U|^{2(r+1)} . \tag{31}$$

This quantity is known as a "frame potential" in the quantum information literature. In general, the structure of $\mathcal{F}_Q$ will depend on $d = p^n$. If we focus on $d = 2^n$ with large n (we will report on the other cases elsewhere [16]), the dimension of the commutant saturates with n to a quantity strictly larger than $(r+1)!$ [17]

$$|\mathcal{F}_{r+1}| = \prod_{k=0}^{r-1} \left(2^k + 1\right) = 2^{r(r-1)/2} \frac{\prod_{k=0}^{\infty} \left(1 + \frac{1}{2^k}\right)}{\prod_{k=0}^{\infty} \left(1 + \frac{1}{2^{k+r}}\right)}, \tag{32}$$

where r can be analytically continued to be a real number in the right-hand side. The statistical mechanics model of monitored Clifford circuits will involve degrees of freedom living in $\mathcal{F}_{r+1}$, which in general has a complicated algebraic structure [17], not relevant to us here. In the limit $n \to \infty$, we expect that the statistical mechanics model reduces once again to a Potts model with $|\mathcal{F}_{r+1}|$ states: this is because any generalization of the Weingarten functions of Haar calculus will become proportional to delta functions in that limit. This is a large D limit, as in the Haar case (except there are different ways to approach this limit in the Clifford case, here we set $D = p^{2n}$ and took $n \to \infty$ with $p = 2$). The central charge as a function of the number of replicas r is now given by $c(r) = 1 - \frac{6}{x(x+1)}$ with $x + 1 = \frac{\pi}{\arccos \frac{\sqrt{|\mathcal{F}_{r+1}|}}{2}}$. This leads to a closed form expression for the effective central charge

$$c_{\text{eff}}^{C, d=2^n \to \infty} = \frac{5\sqrt{3}}{8\pi} \left(2\psi_{\frac{1}{2}} \left(\frac{-i\pi}{\log 2} \right) - \log 8 \right) \simeq 0.365194 \ldots \tag{33}$$

where $\psi_q(z)$ is the q-digamma function, which is defined as the derivative of $\log \Gamma_q(z)$ with respect to z, where $\Gamma_q(z)$ is the q-deformed Gamma function.

[1] B. Efron, in *Breakthroughs in statistics* (Springer, 1992) pp. 569–593.

[2] B. Bertini, P. Kos, and T. Prosen, Phys. Rev. Lett. **123**, 210601 (2019).

[3] Y. Li, X. Chen, and M. P. A. Fisher, Phys. Rev. B **100**, 134306 (2019).

[4] S. Aaronson and D. Gottesman, Phys. Rev. A **70**, 052328 (2004).
[5] M. J. Gullans and D. A. Huse, Phys. Rev. X **10**, 041020 (2020).
[6] J. L. Jacobsen and J. Cardy, Nucl. Phys. B **515**, 701 (1998).
[7] B. Skinner, J. Ruhman, and A. Nahum, Phys. Rev. X **9**, 031009 (2019).
[8] Y. Li, X. Chen, A. W. W. Ludwig, and M. P. A. Fisher, arXiv preprint arXiv:2003.12721 (2020).
[9] M. J. Gullans and D. A. Huse, Phys. Rev. Lett. **125**, 070606 (2020).
[10] R. Fan, S. Vijay, A. Vishwanath, and Y.-Z. You, Phys. Rev. B **103**, 174309 (2021).
[11] R. Vasseur, A. C. Potter, Y.-Z. You, and A. W. W. Ludwig, Phys. Rev. B **100**, 134203 (2019).
[12] C.-M. Jian, Y.-Z. You, R. Vasseur, and A. W. W. Ludwig, Phys. Rev. B **101**, 104302 (2020).
[13] Y. Bao, S. Choi, and E. Altman, Phys. Rev. B **101**, 104301 (2020).
[14] P. Hayden, S. Nezami, X.-L. Qi, N. Thomas, M. Walter, and Z. Yang, J. High Energy Phys. **2016** (11), 9.
[15] T. Zhou and A. Nahum, Phys. Rev. B **99**, 174205 (2019).
[16] Y. Li, R. Vasseur, M. P. A. Fisher, and A. W. W. Ludwig, Statistical mechanics model for clifford random tensor networks and monitored quantum circuits (2021), arXiv:2110.02988 [cond-mat.stat-mech].
[17] D. Gross, S. Nezami, and M. Walter, Commun. Math. Phys. **385**, 1325 (2017).